SUPPORTING INFORMATION

Chinese Journal of Structural Chemistry

S-scheme Porous g-C_3N_4/Ag_2MoO_4 Heterojunction Composite for CO_2 Photoreduction

Zhongliao Wang[1], Ruilian Liu[1], Jinfeng Zhang[1]* and Kai Dai[1]*

[1]*Key Laboratory of Green and Precise Synthetic Chemistry and Applications, Ministry of Education, Anhui Province Key Laboratory of Pollutant Sensitive Materials and Environmental Remediation, School of Physics and Electronic Information, Huaibei Normal University, Huaibei 235000, China*

**Corresponding authors. Fax: +86-561-3803256. Emails: daikai940 @chnu.edu.cn (K. Dai) and jfzhang@chnu.edu.cn (J. Zhang)*

n EXPERIMENTAL

CO_2 Photoreduction Tests. The CO_2 photoreduction test was conducted in a 200 mL quartz reactor with two bottlenecks at ambient temperature. Firstly, 20 mg of the photocatalyst was uniformly dispersed at the bottom of the quartz reactor by adding 10 mL of deionized water with ultrasonication assistance. Then the quartz reactor was transferred into an oven at 80 ^oC to obtain a thin film. After adding 0.1 g of $NaHCO_3$ into the minor groove on the bottleneck, the quartz reactor was sealed and then flowed with N_2 for 0.5 h to generate anaerobic conditions. CO_2 and H_2O vapor were introduced into the reaction system by injecting 0.5 mL of 2 M H_2SO_4 solution to react with $NaHCO_3$ powders. Afterwards, the quartz reactor was positioned under a 300 W solar-simulated Xe arc lamp with a vertical distance of 10 cm. After irradiation for 1 h, 1 mL of gas was drawn from the quartz reactor and then injected into a gas chromatograph (Shimadzu GC-2014C, Japan) with methanizer and flame ionized detector (FID) to analyze its ingredient. The cyclic CO_2 photoreduction tests were conducted as follows: After each CO_2 photoreduction test, the reaction product of H_2SO_4 solution and $NaHCO_3$ is washed. The photocatalyst film was dried again in an oven for the next cyclic test. The rest of the details are the same as the photocatalytic CO_2 test.

Computational Methods. Density functional theory (DFT) calculations were performed using the CP2K-7.1 package. Perdew-Burke-Ernzerh (PBE) of functional was used to describe the system. Unrestricted Kohn-Sham DFT has been used as the electronic structure method in the Gaussian and plane waves (GPW) framework. The Goedecker-Teter-Hutter (GTH) pseudopotentials and Double-ζ molecularly optimized basis sets (DZVP-MOLOPT-GTH) have been used for all elements. A plane-wave energy cutoff of 400 Ry has been employed. The geometries were optimized using the Broyden-Fletcher-Goldfarb-Shanno (BFGS) algorithm, and the convergence criterion for the forces was set to $4.5*10^{-4}$ bohr/hartree. A vacuum layer of 15 Å was constructed to eliminate interactions between periodic structures of surface models. The van der Waals (vdW) interaction was amended by the DFT-D3 method of Grimme.

Table S1. BET Surface Area, Pore Volume, Average Pore Width, and CO_2 Adsorption of AMO, UPCN and UPCN/AMO

Samples	BET surface area ($m^2\ g^{-1}$)	Pore volume ($cm^3\ g^{-1}$)	Average pore width (nm)	CO_2 adsorption μmol g^{-1}
AMO	1.80	0.008	17.8	13.9
UPCN	28.31	0.247	34.9	75.6
UPCN/AMO	16.84	0.083	19.7	25.2

Table S2. Comparison of Various CO_2 Photoreduction Systems

Semiconductor	Cocatalysts	Light source	Conditions	Products	Activity (μmol g^{-1} h^{-1})	Ref. (year)
Bi_2MoO_6/BiOI		300W Xe-lamp	CO_2, H_2O vapor	CO, CH_4	8.34, 3.31	[1] (2022)
Sb/g-C_3N_4		300W Xe-lamp (λ ≥ 420 nm)	CO_2, H_2O vapor	CO	2.03	[2] (2022)
NiO		5 W (400-1000 nm)	$[Ru(bpy)_3]Cl_2·6H_2O$, acetonitrile, H_2O, TEOA, CO_2	CO, H_2	6.28×10^3, 0.14×10^3	[3] (2021)
g-C_3N_4/$Bi_{12}O_{17}Cl_2$		300W Xe-lamp (λ ≥ 420 nm)	CO_2, H_2O vapor	CH_4	24.4	[4] (2021)
Conjugated polymers	Co (II) bipyridine complexes	300W Xe-lamp (λ ≥ 420 nm)	TEOA, H_2O, CO_2	CO	2247	[5] (2020)
TiO_2/C_3N_4	Ti_3C_2-MXene	300W Xe-lamp	CO_2, H_2O vapor	CO, CH_4	4.4, 1.4	[6] (2020)
TiO_2	polydopamine	300W Xe-lamp	CO_2, H_2O vapor	CH_4, CH_3OH	1.50, 0.26	[7] (2021)
BiOBr/NiO		300W Xe-lamp	CO_2, H_2O vapor	CO, CH_4	12.8, 6.6	[8] (2022)
$InVO_4$		300W Xe-lamp	CO_2 vapor, 0.4 mL H_2O solution	CO, CH_4, O_2	18.28, 0.29, 8.5 AQE = 0.54% (385 nm)	[9] (2019)
$CdSe_{0.8}S_{0.2}$-DETA/$SnNb_2O_6$		300W Xe-lamp (λ ≥ 420 nm)	CO_2, H_2O vapor	CO	17.31	[10] (2022)
g-C_3N_4/Sn_2S_3-DETA		300W Xe-lamp (λ ≥ 420 nm)	CO_2, H_2O vapor	CH_4, CH_3OH	4.84, 1.35	[11] (2019)
$InVO_4$/CdSe-DETA		300W Xe-lamp (λ ≥ 420 nm)	CO_2, H_2O vapor	CO	27.9	[12] (2022)
Bi_2S_3/$BiVO_4$/$Mn_{0.5}Cd_{0.5}$S-DETA		300W Xe-lamp (λ ≥ 420 nm)	CO_2, H_2O vapor	CO	44.7	[13] (2022)
TpBpy (Covalent Organic Framework)	Ni single atoms	300W Xe-lamp (λ ≥ 420 nm)	acetonitrile, H_2O, triethanolamine (TEOA), $[Ru(bpy)_3]Cl_2·6H_2O$ filled with CO_2	CO, H_2	811, 34	[14] (2019)
$Cd_xZn_{1-x}Se$/Cu_2O@Cu	Cu	300W Xe-lamp	CO_2, H_2O vapor	CO	50	[15] (2022)
CdS/TiO_2		300W Xe-lamp	CO_2, H_2O vapor	CO, CH_4	17.4, 27.9	[16] (2020)
TiO_2/$CsPbBr_3$		300W Xe-lamp	CO_2, H_2O vapor	CH_4, H_2, O_2	13.49, 0.43, 0.29 AQE: 0.9% (420 nm)	[17] (2020)
MIL-101 filled with TiO_2		300W Xe-lamp	CO_2, H_2O vapor	CO, CH_4, O_2	7.2×10^3, 1×10^3, 7.2×10^3, AQE = 11.3% (350 nm)	[18] (2020)

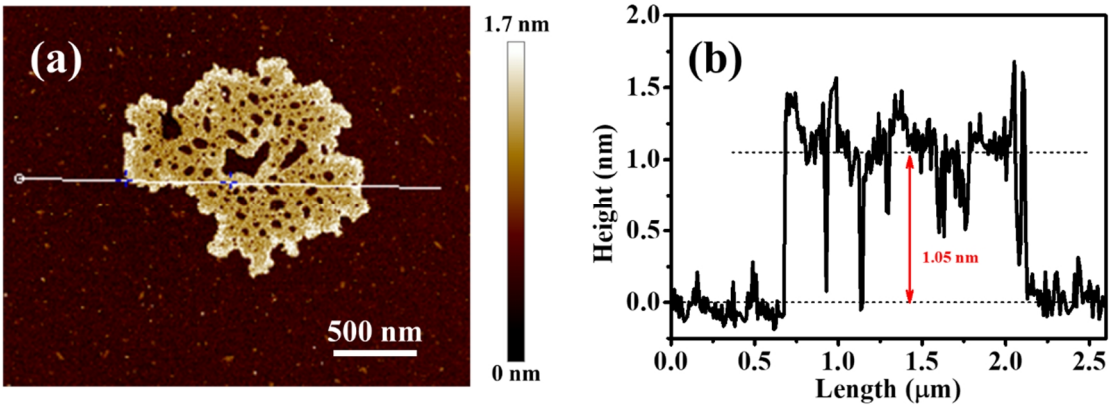

Figure S1. AFM image of UPCN NSs.

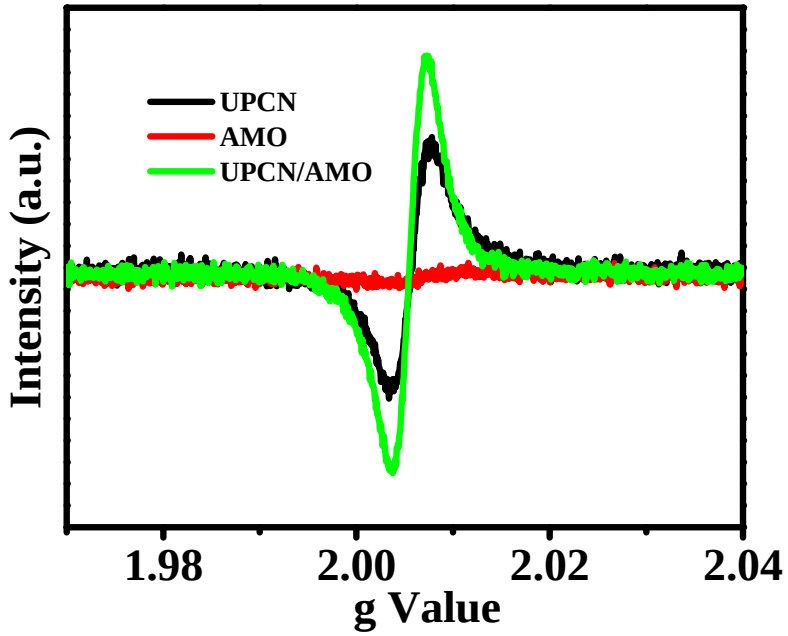

Figure S2. Electron paramagnetic resonance (EPR) spectroscopy of UPCN, AMO and UPCN/AMO composite.

n REFERENCES

(1) Wang, Z.; Cheng, B.; Zhang, L.; Yu, J.; Li, Y.; Wageh, S.; Al-Ghamdi, A. A. S-Scheme 2D/2D Bi_2MoO_6/BiOI van der Waals heterojunction for CO_2 photoreduction. *Chin. J. Catal.* **2022**, 43, 1657-1666.

(2) Zhang, J.; Fu, J.; Dai, K. Graphitic carbon nitride/antimonene van der Waals heterostructure with enhanced photocatalytic CO_2 reduction activity. *J. Mater. Sci. Technol.* **2022**, 116, 192-198.

(3) Chen, W.; Liu, X.; Han, B.; Liang, S.; Deng, H.; Lin, Z. Boosted photoreduction of diluted CO_2 through oxygen vacancy engineering in NiO nanoplatelets. *Nano Res.* **2021**, 14, 730-737.

(4) Huo, Y.; Zhang, J.; Wang, Z.; Dai, K.; Pan, C.; Liang, C. Efficient interfacial charge transfer of 2D/2D porous carbon nitride/bismuth oxychloride step-scheme heterojunction for boosted solar-driven CO_2 reduction. *J. Colloid Interf. Sci.* **2021**, 585, 684-693.

(5) Wang, S.; Hai, X.; Ding, X.; Jin, S.; Xiang, Y.; Wang, P.; Jiang, B.; Ichihara, F.; Oshikiri, M.; Meng, X.; Li, Y.; Matsuda, W.; Ma, J.; Seki, S.; Wang, X.; Huang, H.; Wada, Y.; Chen, H.; Ye, J. Intermolecular cascaded pi-conjugation channels for electron delivery powering CO_2 photoreduction. *Nat. Commun.* **2020**, 11, 1149.

(6) He, F.; Zhu, B.; Cheng, B.; Yu, J.; Ho, W.; Macyk, W. 2D/2D/0D $TiO_2/C_3N_4/Ti_3C_2$ MXene composite S-scheme photocatalyst with enhanced CO_2 reduction activity. *Appl. Catal. B: Environ.* **2020**, 272, 119006.

(7) Meng, A.; Cheng, B.; Tan, H.; Fan, J.; Su, C.; Yu, J. TiO_2/polydopamine S-scheme heterojunction photocatalyst with enhanced CO_2-reduction selectivity. *Appl. Catal. B: Environ.* **2021**, 289, 120039.

(8) Wang, Z.; Cheng, B.; Zhang, L.; Yu, J.; Tan, H. BiOBr/NiO S-Scheme heterojunction photocatalyst for CO_2 photoreduction. *Solar RRL* **2022**, 6, 2100587.

(9) Han, Q.; Bai, X.; Man, Z.; He, H.; Li, L.; Hu, J.; Alsaedi, A.; Hayat, T.; Yu, Z.; Zhang, W.; Wang, J.; Zhou, Y.; Zou, Z. Convincing synthesis of atomically thin, single-crystalline $InVO_4$ sheets toward promoting highly selective and efficient solar conversion of CO_2 into CO. *J. Am. Chem. Soc.* **2019**, 141, 4209-4213.

(10) Yang, H.; Zhang, J. F.; Dai, K. Organic amine surface modified one-dimensional $CdSe_{0.8}S_{0.2}$-diethylenetriamine/two-dimensional $SnNb_2O_6$ S-scheme heterojunction with promoted visible-light-driven photocatalytic CO_2 reduction. *Chin. J. Catal.* **2022**, 43, 255-264.

(11) Huo, Y.; Zhang, J.; Dai, K.; Li, Q.; Lv, J.; Zhu, G.; Liang, C. All-solid-state artificial Z-scheme porous g-C_3N_4/Sn_2S_3-DETA heterostructure photocatalyst with enhanced performance in photocatalytic CO_2 reduction. *Appl. Catal. B: Environ.* **2019**, 241, 528-538.

(12) Mei, F.; Dai, K.; Zhang, J.; Li, L.; Liang, C. Ultrathin indium vanadate/cadmium selenide-amine step-scheme heterojunction with interfacial chemical bonding for promotion of visible-light-driven carbon dioxide reduction. *J. Colloid Interf. Sci.* **2022**, 608, 1846-1856.

(13) Zhao, Z.; Li, X.; Dai, K.; Zhang, J.; Dawson, G. In-situ fabrication of $Bi_2S_3/BiVO_4/Mn_{0.5}Cd_{0.5}S$-DETA ternary S-scheme heterostructure with effective interface charge separation and CO_2 reduction performance. *J. Mater. Sci. Technol.* **2022**, 117, 109-119.

(14) Zhong, W.; Sa, R.; Li, L.; He, Y.; Li, L.; Bi, J.; Zhuang, Z.; Yu, Y.; Zou, Z. A covalent organic framework bearing single Ni sites as a synergistic photocatalyst for selective photoreduction of CO_2 to CO. *J. Am. Chem. Soc.* **2019**, 141, 7615-7621.

(15) Li, X.; Wang, Z.; Zhang, J.; Dai, K.; Fan, K.; Dawson, G. Branch-like $Cd_xZn_{1-x}Se/Cu_2O$@Cu step-scheme heterojunction for CO_2 photoreduction. *Mater. Today Phys.* **2022**, 26, 100729.

(16) Wang, Z.; Chen, Y.; Zhang, L.; Cheng, B.; Yu, J.; Fan, J. Step-scheme CdS/TiO_2 nanocomposite hollow microsphere with enhanced photocatalytic CO_2 reduction activity. *J. Mater. Sci. Technol.* **2020**, 56, 143-150.

(17) Xu, F.; Meng, K.; Cheng, B.; Wang, S.; Xu, J.; Yu, J. Unique S-scheme heterojunctions in self-assembled $TiO_2/CsPbBr_3$ hybrids for CO_2 photoreduction. *Nat. Commun.* **2020**, 11, 4613.

(18) Jiang, Z.; Xu, X.; Ma, Y.; Cho, H. S.; Ding, D.; Wang, C.; Wu, J.; Oleynikov, P.; Jia, M.; Cheng, J.; Zhou, Y.; Terasaki, O.; Peng, T.; Zan, L.; Deng, H. Filling metal-organic framework mesopores with TiO_2 for CO_2 photoreduction. *Nature* **2020**, 586, 549-554.